Asymptotic-Preserving scheme for highly anisotropic non-linear diffusion equations

Andrea Mentrelli Claudia Negulescu

April 3, 2012

Laboratoire d'Analyse Topologie Probabilités (LATP),
Centre de Mathématiques et Informatique (CMI), UMR6632
Université de Provence, Technople Chteau-Gombert,
39, rue F. Joliot Curie, 13453 Marseille Cedex 13, France

e-mail : andrea@cmi.univ-mrs.fr ; claudia.negulescu@cmi.univ-mrs.fr

Abstract

Heat transfer in magnetically confined plasmas is a process characterized by non-linear and extremely high anisotropic diffusion phenomena. Standard numerical methods, successfully employed in the numerical treatment of classical diffusion problems, are generally inefficient, or even prone to break down, when such high anisotropies come into play, leading thus to the need of new numerical techniques suitable for this kind of problems.

In the present paper, the authors propose a numerical scheme based on an asymptotic-preserving (AP) reformulation of this non-linear evolution problem, generalizing the ideas introduced in a previous paper for the case of elliptic anisotropic problems (P. Degond et al., *An asymptotic-preserving method for highly anisotropic elliptic equations based on a Micro–Macro decomposition*, J. Comput. Phys. **231** (2012), no. 7, 2724-2740. The performances of the here proposed AP scheme are tested numerically; in particular it is shown that the scheme is capable to deal with problems characterized by a high degree of anisotropy, thus proving to be suitable for the study of anisotropic diffusion in magnetically confined plasmas.

Keywords: Anisotropic and non-linear diffusion; Asymptotic-Preserving scheme; Magnetically confined plasma simulation.

1 Introduction

Anisotropic non-linear diffusion equations arise in several fields of application and lot of effort is done for an efficient numerical resolution of this kind of challenging problem.

To mention some examples, such non-linear evolution equations of parabolic type occur in the description of an isentropic gas flow through a porous media [2, 19, 29] or in the description of transport phenomena in heterogeneous geologic formations, such as fractured rock systems [6], which are of fundamental interest for petroleum or groundwater engineering. In addition, these equations appear also in image processing, related to the elimination of noise and small-scale details from an image [3, 25, 30] or in the description of the anisotropic water diffusion in tissues of the nervous system [4]. The present paper is closely related to the description of heat diffusion in magnetically confined plasmas [18,21]. This problem, as the previous ones, is characterized by anisotropic diffusion, but the extremely high intensity of the here involved anisotropy somewhat represents a peculiarity which distinguishes this problem and requires a treatment on its own. From a mathematical or computational point of view, several works are concerned with nonlinear/anisotropic diffusion problems, some references being [1, 7, 27, 29].

In the framework of a simplified continuum (fluid) model, the particle temperature T, for each of the two species constituting a magnetically confined plasma (i.e. electrons and ions), is governed by an equation of the type

$$\partial_t T - \frac{1}{\varepsilon}\nabla_{||} \cdot (K_{||} T^{5/2} \nabla_{||} T) - \nabla_\perp \cdot (K_\perp \nabla_\perp T) = 0, \tag{1.1}$$

where ∂_t is the partial derivative with respect to time, the symbols $\nabla_\parallel$ and $\nabla_\perp$, resp. $\nabla_\parallel \cdot$ and $\nabla_\perp \cdot$, represent the gradient, resp. divergence operators in the parallel or perpendicular directions to the confining magnetic field, while $\frac{1}{\varepsilon} K_\parallel T^{5/2}$ and $K_\perp$ represent the corresponding diffusion coefficients. The temperature evolution described by Eq. (1.1) is obtained as part of a model considering the plasma as a low pressure gas obeying the Fourier law and with a negligible viscosity [21]. Despite the strong simplifications that characterize this model, the temperature equation introduced above contains much of the physics peculiar to a magnetically confined plasma: it accounts for the anisotropy feature of the heat diffusion phenomena, and it clearly points out the role played by the magnetic field, being able to greatly affect the temperature distribution in the plasma. This is translated by the fact that the directions parallel and perpendicular to the magnetic field are characterized by diffusion coefficients that vary by several orders of magnitude. In the framework of the present model, $K_\parallel$ and $K_\perp$ are of the same order of magnitude, while ε is a small parameter which is responsible for the high anisotropy of the diffusion process (in physically relevant situations, one typically has $0 < \varepsilon \ll 1$) [20]. Moreover, it should also be stressed that Eq. (1.1) is non-linear, the parallel diffusion coefficient being proportional to $T^{5/2}$.

From a physical point of view, the reason for such a high anisotropic diffusion process is due to the magnetic confinement. Indeed, the purpose of the magnetic field is to restrict the particle motion across, but not along the magnetic field lines, thus singling out transport phenomena along the parallel direction. The direct consequences of this magnetic confinement are small resistivities along the field lines and an extremely large ratio of parallel to perpendicular thermal conductivities.

When high anisotropies are involved, all the standard numerical methods developed so far break down or are highly inefficient [15]; in order to catch and to preserve the highly anisotropic feature of the diffusion process, it is typically required to adopt severe time-step and mesh-size constraints and/or to use a computational mesh which takes

into account the direction of the anisotropy, i.e. of the magnetic field itself. Since for a variety of reasons it is desirable to avoid such limitations, it is of primary importance to develop numerical techniques that can be successfully applied to the resolution of Eq. (1.1) irrespective of the degree of the anisotropy and exploitable on a simple Cartesian mesh.

An efficient and performant fast semi-implicit method has been recently developed [27], in a framework similar to the subject of the present paper, however with the important difference that the problem there is linear, anisotropic but not singularly perturbed. The range of validity of the there developed method is limited – at least in the formulation proposed so far – as it considers only a fixed ε, and is hence inapplicable in the limit $\varepsilon \to 0$ and thus inapplicable for variable anisotropies within the domain of interest.

To overcome all the limitations affecting the standard numerical methods, it is at first necessary to understand why these methods are inefficient (or not even applicable) in case of highly anisotropic diffusion. The main reason is connected to the fact that the original problem – written in terms of Eq. (1.1) – is a so-called *singular perturbation* (SP) problem, meaning that in the limit $\varepsilon \to 0$ its solutions converge to the solutions of a *limit problem* which typically is *qualitatively* different (because of a change in type or nature of the original model equations) from the original singular perturbation problem. A successful approach in developing efficient numerical methods for solving these kind of problems is based on the idea of reformulating the original SP problem, with the aim of obtaining an equivalent regular problem, i.e. a formulation which appears as a regular perturbation of the limit problem, thus avoiding the singularity when $\varepsilon \to 0$. Such an *asymptotic-preserving* (AP) reformulation of the original SP problem (if it exists) turns out to be treatable with standard numerical methods (for instance, by means of the finite element methods) irrespective of the value of the perturbation parameter ε [15].

Initially, this kind of asymptotic-preserving technique was introduced by S. Jin in the framework of the numerical resolution of multiscale kinetic equations [23]. Later on, several other works have developed AP techniques for multiscale kinetic models [5,10,24] as well as fluid models [8, 9, 15, 16], the reference list being not exhaustive.

The purpose of the present paper is hence the introduction of an AP scheme in the framework of the non-linear, highly anisotropic evolution problem (1.1). A semi-discretization in time and a linearization via a fixed point map will lead to an anisotropic elliptic problem, which shall be reformulated in AP form following the procedure already developed for elliptic linear problems [17]. The novelty of this work is the design of an AP scheme in a non-linear setting. The focus will be the validation of the here developed method, in particular its asymptotic preserving property, as well as its application to the specific case of the temperature evolution in a magnetically confined plasma; a detailed mathematical and numerical analysis of the proposed method is left as the subject of a forthcoming paper.

It should however be stressed that the method proposed here is completely general and its range of application is not restricted to fusion plasma simulation. Since the method, in contrast to other recently developed methods (as [27]), does not assume that the diffusion is aligned with one coorinate axis, it could find applications also in problems in which the diffusion direction is arbitrary, or in problems in which the degree

of anisotropy varies (possibly of several orders of magnitude) over the computational domain (even if the perturbation parameter ε will be considered constant in the following, the method is quite more general and there is no need for such an assumption).

The paper is organized as follows. In Section 2, the non-linear evolution problem of the temperature distribution in magnetically confined plasmas is introduced. In Section 3, the numerical method proposed for the resolution of this evolution problem is detailed: the semi-discretization in time as well as the treatment of the non-linearity are illustrated in Section 3.1; the semi-discretization in space and the procedure that leads to the reformulation of the original SP problem in its AP form are detailed in Section 3.2. The description of the numerical tool that has been developed and the discussion of some numerical results are provided in Section 4. The validation of the proposed AP scheme is presented in two reference cases for which analytical solutions of the non-linear evolution problem and also of the corresponding non-linear elliptic problem, have been expressly constructed (Section 4.1). The comparison of the results obtained by means of the AP scheme to those obtained by means of standard techniques is the subject of Section 4.2. Section 4.3 deals with a selection of the numerical results obtained when the proposed AP scheme is applied to the specific problem presented in Section 2. Finally, in Section 5 some conclusions regarding the effectiveness and the efficiency of the application of the AP scheme to the numerical resolution of the non-linear evolution problem are drawn.

2 Description of the problem

We consider a two or three dimensional anisotropic, non-linear heat problem, given on a sufficiently smooth, bounded domain $\Omega \subset \mathbb{R}^d$, $d = 2, 3$ with boundary Γ. The direction of the anisotropy is defined by the time-independent vector field $b \in (C^\infty(\Omega))^d$, satisfying $|b(x)| = 1$ for all $x \in \Omega$.

Given this vector field b, one can decompose a vector $v \in \mathbb{R}^d$, its divergence $\nabla \cdot v$, and the gradient $\nabla\phi$ of a scalar function $\phi(x)$ into a component parallel to the anisotropy direction and a component perpendicular to it:

$$
\begin{aligned}
&v_{||} := (v \cdot b)b\,, && v_\perp := (\mathbb{I} - b \otimes b)v\,, && \text{such that} \quad v = v_{||} + v_\perp\,,\\
&\nabla_{||} \cdot v := \nabla \cdot v_{||}\,, && \nabla_\perp \cdot v := \nabla \cdot v_\perp\,, && \text{such that} \quad \nabla \cdot v = \nabla_{||} \cdot v + \nabla_\perp \cdot v\,,\\
&\nabla_{||}\phi := (b \cdot \nabla\phi)b\,, && \nabla_\perp\phi := (\mathbb{I} - b \otimes b)\nabla\phi\,, && \text{such that} \quad \nabla\phi = \nabla_{||}\phi + \nabla_\perp\phi\,,
\end{aligned}
$$

where $\otimes$ is the vector tensor product and $\mathbb{I}$ is the $d \times d$ identity matrix. The boundary Γ can be decomposed into three parts following the sign of the intersection with b:

$$
\Gamma_D := \{x \in \Gamma \ / \ b(x) \cdot n(x) = 0\}, \quad \Gamma_{in} := \{x \in \Gamma \ / \ b(x) \cdot n(x) < 0\}\,,
$$

$$
\Gamma_{out} := \{x \in \Gamma \ / \ b(x) \cdot n(x) > 0\}, \quad \Gamma_N = \Gamma_{in} \cup \Gamma_{out}
$$

where the vector n is here the unit outward normal on Γ.

With these notations, the problem introduced in Eq. (1.1) can be written, along with its proper boundary and initial conditions, as follows:

$$(P)\quad \begin{cases} \partial_t T - \dfrac{1}{\varepsilon}\nabla_{||}\cdot(K_{||}T^{5/2}\nabla_{||}T) - \nabla_{\perp}\cdot(K_{\perp}\nabla_{\perp}T) = 0\,, & \text{in} \quad [0,S]\times\Omega\,, \\ \dfrac{1}{\varepsilon}n_{||}\cdot(K_{||}T^{5/2}(t,\cdot)\nabla_{||}T(t,\cdot)) + n_{\perp}\cdot(K_{\perp}\nabla_{\perp}T(t,\cdot)) = & -(\gamma-5/2)T(t,\cdot)\,, \\ & \text{on} \quad [0,S]\times\Gamma_N\,, \\ \nabla_{\perp}T(t,\cdot) = 0\,, & \text{on} \quad [0,S]\times\Gamma_D\,, \\ T(0,\cdot) = T_0(\cdot)\,, & \text{in} \quad \Omega\,. \end{cases} \tag{2.2}$$

As pointed out in Section 1, the function T represents the temperature of the ions/electrons, $K_{||}$ and $K_{\perp}$ are two coefficients of the same order of magnitude and ε is a (typically very small) positive parameter ($0 < \varepsilon \ll 1$). The coefficient γ represents the sheath heat transmission coefficients and takes the value $\gamma = 9/2$ for the ions, resp. $\gamma = 5/2$ for the electrons [28], and $[0,S]$ is the time interval over which the temperature evolution is to be studied, starting from a given initial temperature distribution T_0.

It is worth observing that the boundary conditions $(2.2)_{2,3}$ correspond, in the case of ions ($\gamma = 9/2$), to a null or outgoing energy flux (respectively, on Γ_D and Γ_N) and, in the case of electrons ($\gamma = 5/2$), to a null flux on the whole boundary Γ.

The parameter $0 < \varepsilon \ll 1$ can be very small and is responsible for the high anisotropy of the problem. The numerical difficulty in solving (2.2) comes from the fact that letting $\varepsilon \to 0$ in (2.2) leads to the reduced problem

$$(R)\quad \begin{cases} -\nabla_{||}\cdot(K_{||}T^{5/2}\nabla_{||}T) = 0\,, & \text{in} \quad [0,S]\times\Omega\,, \\ n_{||}\cdot(K_{||}T^{5/2}(t,\cdot)\nabla_{||}T(t,\cdot)) = 0\,, & \text{on} \quad [0,S]\times\Gamma_N\,, \\ \nabla_{\perp}T(t,\cdot) = 0\,, & \text{on} \quad [0,S]\times\Gamma_D\,, \\ T(0,\cdot) = T_0(\cdot)\,, & \text{in} \quad \Omega\,. \end{cases} \tag{2.3}$$

which is an ill-posed problem admitting an infinite amount of solutions, if T_0 satisfies $(2.3)_1$, or no solution in the contrary case. To avoid this problem, standard numerical schemes adapt the time- and space-grids to ε, when solving (2.2), which leads to extremely high computational costs, if $0 < \varepsilon \ll 1$. From a computational point of view, the ill-posedness of the reduced problem (2.3), is translated in an ill-conditioned linear system to be solved for the solution of (2.2) when $0 < \varepsilon \ll 1$.

The aim of this paper is to introduce an efficient numerical method permitting to solve (2.2) on a coarse Cartesian mesh, which has not to be adapted to the field lines of b and whose mesh size is independent on the value of ε. To this aim, we shall study a test case, with an initial temperature T_0 consisting of a hot spot (see Fig. 1) and analyze the diffusion process, paying attention to the numerical diffusion perpendicularly to the magnetic field lines.

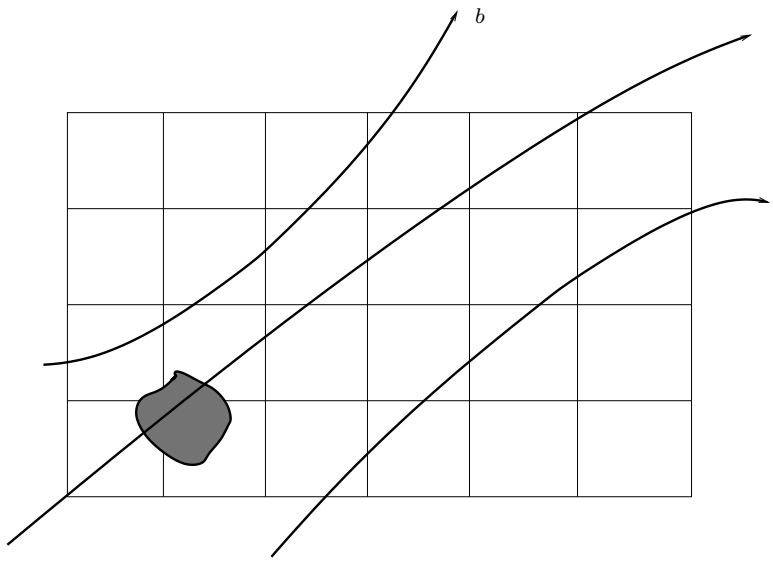

Figure 1: Sketch of the computational domain, of the magnetic field and of the initial hot spot.

We shall assume in the rest of this paper the following mathematical hypothesis.

Hypothesis A *Let* $\overset{\circ}{\Gamma}_D \neq \varnothing$, $T_0 \in L^2(\Omega)$, $T_0 \geqslant 0$ *and suppose* $0 < \varepsilon \ll 1$, $\gamma \geqslant 5/2$ *fixed. The diffusion coefficients* $K_\parallel \in L^\infty(\Omega)$ *and* $K_\perp \in \mathbb{M}_{d\times d}(L^\infty(\Omega))$ *are supposed to satisfy*

$$0 < K_0 \leqslant K_\parallel(x) \leqslant K_1\,, \quad \textit{f.a.a. } x \in \Omega,$$

$$K_0||v||^2 \leqslant v^t K_\perp(x) v \leqslant K_1||v||^2\,, \quad \forall v \in \mathbb{R}^d \textit{ and f.a.a. } x \in \Omega,$$

with $0 < K_0 \leqslant K_1$ *some constants.*

3 Numerical discretization

Let us introduce in this section the Asymptotic-Preserving numerical method we developed. Firstly we shall discretize the equation (2.2) in time and linearize the problem. Then an AP-strategy is adopted to discretize in space the obtained highly anisotropic elliptic problem. For the sake of simplicity, but with no loss in generality, we shall consider only the case of a 2D rectangular domain $\Omega := [0, L_x] \times [0, L_y]$, the generalization to the 3D case being straightforward.

The following symbols concerning the homogeneous discretization of the time and space domains are adopted:

$$\begin{aligned}
&0 = t_0 < t_1 < \cdots < t_{N_t} = S, && t_n = n\Delta t, \quad n = 0, \ldots, N_t,\\
&0 = x_1 < x_2 < \cdots < x_{N_x} = L_x, && x_i = (i-1)\,\Delta x, \quad i = 1, \ldots, N_x,\\
&0 = y_1 < y_2 < \cdots < y_{N_y} = L_y, && y_j = (j-1)\,\Delta y, \quad j = 1, \ldots, N_y,
\end{aligned}$$

where $\Delta t = S/N_t$, $\Delta x = L_x/(N_x - 1)$ and $\Delta y = L_y/(N_y - 1)$ are, respectively, the time and space steps. We shall denote in the following by T_{ij}^n the approximation of the temperature in the point (x_i, y_j) of the domain Ω at time t_n.

To simplify the notations, we shall also introduce, for a fixed Φ, the diffusion operator $L(\Phi)$ defined by

$$L(\Phi)T := -\frac{1}{\varepsilon}\nabla_{||} \cdot (K_{||}\Phi^{5/2}\nabla_{||}T) - \nabla_{\perp} \cdot (K_{\perp}\nabla_{\perp}T).$$

3.1 Semi-discretization in time and treatment of the non-linearity

The first step in the treatment of $(2.2)_1$ consists in the semi-discretization in time via the Euler implicit method. This leads to the following sequence of equations:

$$\frac{T^{n+1} - T^n}{\Delta t} + L(T^{n+1})T^{n+1} = 0\,, \quad n = 0, \cdots, N_t - 1\,. \tag{3.4}$$

As one can observe, we have to deal, for each fixed n, with a non-linear equation. To solve this one, a fixed point argument is used. For fixed $n \in \mathbb{N}$, let us start our iterative procedure by setting $T^{n,0} := T^n$ and construct the iterative sequence by associating to $T^{n,k}$ the solution $T^{n,k+1}$ of the following linear equation

$$\frac{T^{n,k+1} - T^n}{\Delta t} + L\left(T^{n,k}\right)T^{n,k+1} = 0, \tag{3.5}$$

completed with the corresponding boundary conditions. The Schauder fixed point theorem allows to show that the sequence $\{T^{n,k}\}_k$ converges towards the unique fixed point, which is T^{n+1}, solution of (3.4).

The proof of the convergence of the fixed-point sequence $T^{n,k}$ is left for a forthcoming, more mathematically-oriented paper. For the time being, we restrict ourselves to reporting that in all the computations performed so far, the convergence of the sequence has always been reached (within the chosen numerical tolerance $\epsilon_{tol} = 10^{-6}$) after a number of steps typically less than 10. Denoting by k^* the number of steps required to reach the convergence of the sequence, in the sens:

$$\begin{aligned} &\|T^{n,k} - T^{n,k-1}\|_{L^2} > \epsilon_{tol}, \quad 0 < k < k^* \\ &\|T^{n,k^*} - T^{n,k^*-1}\|_{L^2} \leqslant \epsilon_{tol}, \end{aligned}$$

the behavior of k^* as a (discrete) function of the time index n, for three different sizes of the time interval Δt ($\Delta t = 10^{-6}$, $\Delta t = 10^{-7}$ and $\Delta t = 10^{-8}$), in a reference case which may be assumed as representative of all the calculations performed so far ($\varepsilon = 10^{-6}$, $N_x \times N_y = 64$), is shown in Fig. 2. The dependence of the number of steps required to reach convergence, k^*, is not markely affected by the mesh size: a larger number of grid points (i.e. of N_x and N_y) leads to smaller values of k^* in the earlier stage of the transient (i.e. for *small* values of n); then, as the system evolves towards the equilibrium state (i.e. for *large* values of n), the values of k^* quickly attains its minimum value and no further reduction of k^* is obtainable adopting more refined meshes.

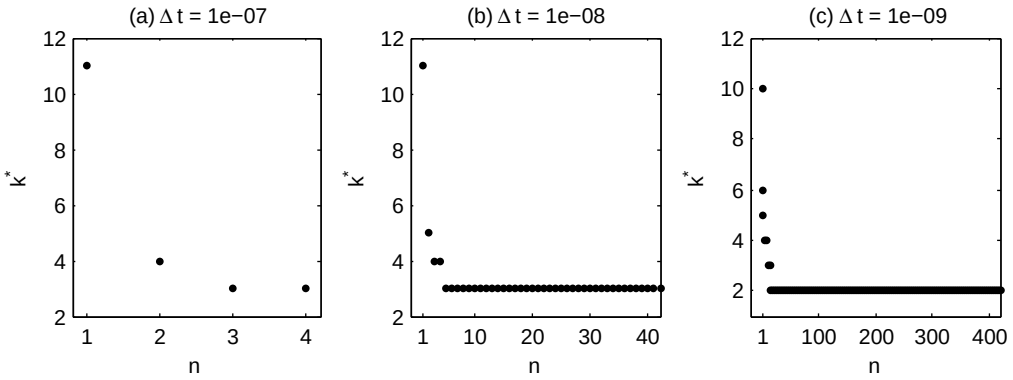

Figure 2: Number of required steps, k^*, to reach the convergence of the sequence $T^{n,k}$ as a (discrete) function of the time step n, for $\varepsilon = 10^{-6}$, $N_x \times N_y = 64$, and three different Δt: (a) $\Delta t = 10^{-6}$; (b) $\Delta t = 10^{-7}$; (c) $\Delta t = 10^{-8}$.

3.2 Semi-discretization in space: application of the AP methodology

The linearized equation (3.5) is a highly anisotropic elliptic equation, to be solved several times at each time step n. To this aim, the Asymptotic-Preserving scheme introduced in [17] can be profitably adopted.

In order to simplify the presentation and also to keep the same notations as in [17], we shall denote the unknown $T^{n,k+1}$ by Θ and put $A_{||} := K_{||}(T^{n,k})^{5/2}$, $A_\perp := K_\perp$, which are known functions.

At this stage, the system that we have to solve for each n is the following:

$$\begin{cases} \Theta - \frac{\Delta t}{\varepsilon}\nabla_{||}\cdot(A_{||}\nabla_{||}\Theta) - \Delta t\nabla_\perp\cdot(A_\perp\nabla_\perp\Theta) = T^n\,, \quad \text{in} \quad \Omega\,, \\ \frac{1}{\varepsilon}n_{||}\cdot(A_{||}\nabla_{||}\Theta) + n_\perp\cdot(A_\perp\nabla_\perp\Theta) = -(\gamma-5/2)\Theta\,, \quad \text{on} \quad \Gamma_N\,, \\ \nabla_\perp\Theta = 0\,, \quad \text{on} \quad \Gamma_D\,. \end{cases} \tag{3.6}$$

Defining now the bilinear forms

$$a_{||}(\Theta,\chi) := \int_\Omega A_{||}\nabla_{||}\Theta\cdot\nabla_{||}\chi\,dx\,, \quad a_\perp(\Theta,\chi) := \int_\Omega A_\perp\nabla_\perp\Theta\cdot\nabla_\perp\chi\,dx\,,$$

on the Hilbert space

$$\mathcal{V} := \{\Phi\in H^1(\Omega)\,/\,\Phi|_{\Gamma_D}=0\}, \qquad (\Phi,\Psi)_{\mathcal{V}} := \left(\nabla_\parallel\Phi,\nabla_\parallel\Psi\right)_{L^2(\Omega)} + \varepsilon\left(\nabla_\perp\Psi,\nabla_\perp\Psi\right)_{L^2(\Omega)}\,,$$

and letting moreover $\mathcal{L}$ be the Hilbert space given by

$$\mathcal{L} := \{\lambda\in L^2(\Omega)\,/\,\nabla_\parallel\lambda\in L^2(\Omega)\,,\ \lambda|_{\Gamma_{in}}=0\}, \qquad (\lambda,\mu)_{\mathcal{L}} := \left(\nabla_\parallel\lambda,\nabla_\parallel\mu\right)_{L^2(\Omega)}\,,$$

we can introduce the weak formulation of (3.6): Find $\Theta\in\mathcal{V}$, solution of

$$(SP) \qquad (\Theta,\chi)_{L^2(\Omega)} + \frac{\Delta t}{\varepsilon}\,a_{||}(\Theta,\chi) + \Delta t\,a_\perp(\Theta,\chi) + \Delta t\,(\gamma-5/2)\int_{\Gamma_N}\Theta\chi\,d\sigma = (T^n,\chi)_{L^2(\Omega)}, \quad \forall\chi\in\mathcal{V}.$$

This is a highly anisotropic problem, which gets ill-posed in the limit $\varepsilon \to 0$. Introducing now, as proposed in [17], the decomposition $\Theta = P + \varepsilon Q$, with $\nabla_{||}\Theta = \varepsilon \nabla_{||} Q$, then one gets the following AP reformulation of the SP problem:

$$(AP) \quad \begin{cases} (\Theta,\chi)_{L^2(\Omega)} + \Delta t\, a_{||}(Q,\chi) + \Delta t\, a_{\perp}(\Theta,\chi) + \Delta t\,(\gamma - 5/2) \displaystyle\int_{\Gamma_N} \Theta\chi\, d\sigma = \\ \qquad\qquad\qquad\qquad\qquad\qquad\qquad\qquad (T^n,\chi)_{L^2(\Omega)}, \qquad \forall \chi \in \mathcal{V} \\ a_{||}(\Theta,\xi) - \varepsilon a_{||}(Q,\xi) = 0\,, \qquad\qquad\qquad\qquad\qquad\qquad \forall \xi \in \mathcal{L}. \end{cases} \tag{3.7}$$

which has the crucial advantage of being well-posed in the limit $\varepsilon \to 0$, in contrast to the ill-posedness of the (SP)-problem. Indeed, putting formally $\varepsilon = 0$ in (3.7) yields a well-posed saddle-point problem, where the unknown Q acts as a Lagrangian. Let us underline, that in the limit $\varepsilon \to 0$ the unknown Q will not vanish, and it is this Q which forces the uniqueness of the solution, as we do not loose any more the information about the perpendicular direction, as it was the case in (2.3). This property of well-posedness in the limit, permits to get precise results, choosing coarse homogeneous meshes, independent of the anisotropy direction and independent on the intensity of the anisotropy. The detailed mathematical study is available in [17].

3.3 From the AP reformulation to the discretized equations

The system of continuous equations (3.7) will be solved numerically via a finite element method (FEM), which seems quite natural because of the weak formulation of the equations appearing in the system.

The computational (polyhedric or polygonal) domain Ω is subdivided into a set of N_e non-overlapping polyhedric (or polygonal) subdomains Ω_h such that $\Omega = \bigcup_{i=1}^{N_e} \Omega_h$ and the vertex of one subdomain lies on the face (edge) of some other subdomain[1]. The overall number of subdomain vertices will be denoted in the following by M. In the case of a 2D quadrilateral domain Ω discretized by means of a Cartesian grid as discussed in Section 3 and subdivided in triangular subdomains Ω_i, we have $N_e = 2\,(N_x - 1)\,(N_y - 1)$ and $M = N_x \times N_y$. Let us moreover denote by $\mathcal{I}$ the set of vertex numbers, belonging to the domain boundary Γ_{in}.

After introducing the $\mathcal{P}_1$-*form functions* φ_i (see, for example, [22]) we approximate the infinite dimensional spaces $\mathcal{V}$ and $\mathcal{L}$ by

$$\mathcal{V}_h := \{v_h := \sum_{i=1}^{M} v_i \varphi_i\}\,, \quad \mathcal{L}_h := \{l_h \in \mathcal{V}_h \;/\; l_{h|\Gamma_{in}} = 0\} = \{l_h := \sum_{k=1, k\notin\mathcal{I}}^{M} l_k \varphi_k\}\,,$$

and we are searching for the unknown functions $(\Theta_h, Q_h) \in \mathcal{V}_h \times \mathcal{L}_h$, solutions of the

[1]Since no attempt is made here to provide a general description of FEM, we are assuming that Ω is a polyhedric (in the 3D case) or polygonal (in the 2D case) domain and that $\Omega_i, \Omega_2, \ldots, \Omega_{N_e}$ are polyhedric (or polygonal) subdomains. More general cases are typically considered in textbooks.

following discrete system

$$(AP)_h \quad \begin{cases} (\Theta_h, \chi_h)_{L^2(\Omega)} + \Delta t\, a_{||}(Q_h, \chi_h) + \Delta t\, a_{\perp}(\Theta_h, \chi_h) + \Delta t\,(\gamma - 5/2) \displaystyle\int_{\Gamma_N} \Theta_h \chi_h \, d\sigma = \\ \qquad\qquad (T^n, \chi_h)_{L^2(\Omega)}, \qquad \forall \chi_h \in \mathcal{V}_h \\ a_{||}(\Theta_h, \xi_h) - \varepsilon a_{||}(Q_h, \xi_h) = 0\,, \qquad \forall \xi_h \in \mathcal{L}_h. \end{cases} \tag{3.8}$$

Inserting now in this system the decomposition

$$\Theta_h = \sum_{j=1}^{M} \Theta_j \varphi_j\,, \quad Q_h = \sum_{l=1, l\notin\mathcal{I}}^{M} Q_l \varphi_l\,,$$

and taking as test functions $\chi_h := \varphi_i$ as well as $\xi_h := \varphi_k$, yields the linear system to be solved at each time step

$$\begin{pmatrix} A & B \\ C & D \end{pmatrix} \begin{pmatrix} \Theta_j \\ Q_l \end{pmatrix} = \begin{pmatrix} F_i \\ 0 \end{pmatrix},$$

with $i, j = 1, \cdots, M$ and $k, l = 1, \cdots, M$ where $k, l \notin \mathcal{I}$. Moreover

$$A_{ij} := (\varphi_j, \varphi_i)_{L^2(\Omega)} + \Delta t\, a_{\perp}(\varphi_j, \varphi_i) + \Delta t\,(\gamma - 5/2) \int_{\Gamma_N} \varphi_j \varphi_i \, d\sigma\,, \quad B_{il} := \Delta t\, a_{||}(\varphi_l, \varphi_i)$$

$$C_{kj} := a_{||}(\varphi_j, \varphi_k)\,, \quad D_{kl} := a_{||}(\varphi_l, \varphi_k)\,, \quad F_i := (T^n, \varphi_i)_{L^2(\Omega)}$$

The resolution of this linear system permits to compute the solution $T^{n,k+1}$ corresponding to the fixed point map (3.5), and after an interative procedure to solve finally the semi-discrete system (3.4).

4 Numerical results

In order to solve numerically the temperature evolution problem (2.2) via the AP scheme described in Section 3, a program which allow to solve the following, slightly more general problem has been designed and implemented:

$$\begin{cases} \partial_t T - \nabla \cdot \mathbb{K} \nabla T = f & \text{in } [0, S] \times \Omega, \\ \alpha_{in}\,(n \cdot \mathbb{K} \nabla T) + \beta_{in} T = \gamma_{in} & \text{on } [0, S] \times \Gamma_{in}, \\ \alpha_{out}\,(n \cdot \mathbb{K} \nabla T) + \beta_{out} T = \gamma_{out} & \text{on } [0, S] \times \Gamma_{out}, \\ \alpha_D\,(n \cdot \mathbb{K} \nabla T) + \beta_D T = \gamma_D & \text{on } [0, S] \times \Gamma_D, \\ T\,(0, \cdot) = T_0\,(\cdot) & \text{in } \{0\} \times \Omega, \end{cases} \tag{4.9}$$

where $\mathbb{K}$ denotes the diffusion matrix defined as follows:

$$\mathbb{K} = \frac{1}{\varepsilon} \mathcal{K}_{\|} b \otimes b + (\mathbb{I} - b \otimes b)\, \mathcal{K}_{\perp}\, (\mathbb{I} - b \otimes b)\,,$$

$\mathcal{K}_{\|}$ is a positive scalar field representing the diffusion coefficient along the *parallel direction* (i.e. the direction parallel to the magnetic field, whose versor has already been

defined as b) and $\mathcal{K}_\perp$ is a symmetric positive definite matrix accounting for the diffusion process along the perpendicular directions. Remark that, there is no restriction for $\mathcal{K}_\parallel$ and $\mathcal{K}_\perp$ to be constants; non-linear problems may be treated as well as linear ones.

In its present form, the program allows to treat general two-dimensional domains Ω and its object-oriented structure allows a straightforward generalization to the case of three dimensions. The discretization of the domain may be made by means of structured as well as unstructured meshes, thus permitting to deal effectively with domains Ω delimited by boundaries Γ of any shape. Nevertheless, specialized versions of the computational routines have been developed in order to deal as efficiently as possible with the specific case of two-dimensional rectangular domains Ω discretized by means of structured meshes. Since the aim of the present paper is to test the AP scheme, in particular its asymptotic preserving property on simple grids, and to compare it with classical methods, we shall restrict ourselves to solving the governing equations of our problem on two-dimensional rectangular domains Ω discretized via uniform (structured) Cartesian meshes, as depicted in Section 3.

It is worth mentioning that, despite the fact that the code allows the user to set mixed boundary conditions on each of the portions Γ_{in}, Γ_{out} and Γ_D of the boundary, the case of interest in the present analysis (i.e. the problem described in Eq. (2.2)) is obtained by setting the following parameters in $(4.9)_{2,3,4}$:

$$\alpha_{in} = \alpha_{out} = \alpha_D = 1, \quad \beta_{in} = \beta_{out} = \gamma - 5/2, \quad \beta_D = \gamma_{in} = \gamma_{out} = \gamma_D = 0, \tag{4.10}$$

and by setting the scalar field $\mathcal{K}_\parallel$, the matrix field $\mathcal{K}_\perp$ and the source term f as follows:

$$\mathcal{K}_\parallel = K_\parallel T^{5/2}, \qquad \mathcal{K}_\perp = K_\perp \mathbb{I}, \qquad f = 0. \tag{4.11}$$

Under these assumptions, the problem described in Section 2 is fully recovered.

Among its options, the program allows even the user to solve an elliptic version of system (4.9), i.e. it is also capable to solve the following problem:

$$\begin{cases} -\nabla \cdot \mathbb{K}\nabla T = f & \text{in } \Omega, \\ \alpha_{in}\,(n \cdot \mathbb{K}\nabla T) + \beta_{in} T = \gamma_{in} & \text{on } \Gamma_{in}, \\ \alpha_{out}\,(n \cdot \mathbb{K}\nabla T) + \beta_{out} T = \gamma_{out} & \text{on } \Gamma_{out}, \\ \alpha_D\,(n \cdot \mathbb{K}\nabla T) + \beta_D T = \gamma_D & \text{on } \Gamma_D. \end{cases} \tag{4.12}$$

We shall refer to the problem defined by Eq. (4.12) as the *steady problem*, whereas the problem defined by Eq. (4.9) is addressed as the *evolution problem*.

It is easily seen that, in the case of constant fields $\mathcal{K}_\parallel$ and $\mathcal{K}_\perp$ (for instance: $\mathcal{K}_\parallel = 1$ and $\mathcal{K}_\perp = \mathbb{I}$) , and with the following choice of the coefficients appearing in Eq. (4.12):

$$\alpha_{in} = \alpha_{out} = \beta_D = 1, \quad \alpha_D = \beta_{in} = \beta_{out} = \gamma_{in} = \gamma_{out} = \gamma_D = 0,$$

the problem being solved replicates the linear elliptic one discussed in [17].

Both the evolution and steady problems are numerically solved via the AP formulation, making use of the finite element method. Nevertheless, the SP formulation associated to both problems has also been solved in a number of reference cases, mainly

for comparison purposes with the results obtained by means of the AP formulation (see Section 4.2).

In all the results presented in the following, the evolution of the temperature has been calculated on a rectangular domain $\Omega = [0,1] \times [0,1]$ discretized by means of triangular elements ($\mathcal{P}_1$-elements) obtained via a uniform Cartesian grid based on a $N_x \times N_y$ discretization of the domain.

The numerical integration required in the discretization process has been tackled by means of the Gauss-Legendre quadrature rules with six couples of nodes and weights. No appreciable improvement has been noted when using a larger number of nodes/weights.

The systems of linear equations resulting from the discretization of the equations have been solved by means of a direct method (via LU factorization), making use of the routines optimized for sparse matrices included in the UMFPACK library [11–14].

All the calculations have been carried out on a machine equipped with an Intel Xeon X5570 processor and 24 GB of RAM memory in the IEEE double precision floating-point format.

4.1 Validation of the AP scheme

The first step is to validate the numerical scheme based on the asymptotic-preserving (AP) reformulation, in particular its convergence with respect to the time and space mesh-sizes and for fixed ε-value. For this, an analysis of its performances is done in two reference cases, for which analytical solutions to a non-linear time-dependent problem of the form (4.9) and to a non-linear steady problem of the form (4.12) are known. Section 4.2 will be concerned with the more important part, which is the study of the asymptotic preserving property of the scheme, when $\varepsilon \to 0$.

Comparison of the numerical results with a time-dependent exact solution

As a first step, the numerical results obtained via the AP scheme of Section 3 are compared to a corresponding non-linear, time-dependent exact solution of problem (4.9), constructed in the following manner. Assuming the magnetic field b aligned with the x-axis, and taking as source term f the function

$$\begin{aligned} f =& c_2 \exp(c_3 t)\, K_\perp \pi^2 (1 + \varepsilon \cos(2\pi x)) \sin(\pi y) - \\ & c_3 \exp(c_3 t) (c_1 + c_2 (1 + \varepsilon \cos(2\pi x)) \sin(\pi y)) - \\ & 10 c_2^2 K_\parallel \pi^2 \varepsilon \sin^2(2\pi x) \sin^2(\pi y) (\exp(-c_3 t) (c_1 + c_2 (1 + \varepsilon \cos(2\pi x)) \sin(\pi y)))^{3/2} + \\ & 4 c_2 \exp(c_3 t)\, K_\parallel \pi^2 \cos(2\pi x) \sin(\pi y) (\exp(-c_3 t) (c_1 + c_2 (1 + \varepsilon \cos(2\pi x)) \sin(\pi y)))^{5/2} \end{aligned}$$

equation (4.9) admits the following solution:

$$T = (c_1 + c_2 (\sin(\pi y) + \varepsilon \cos(2\pi x) \sin(\pi y))) \exp(-c_3 t), \tag{4.13}$$

where c_1, c_2, c_3 and ε are parameters.

The L^2- and H^1-norms of the errors between the numerical resolutions and the exact solution at $t = 0.1$ are given in Table 1 for various space mesh-sizes and with a fixed

time step $\Delta t = 10^{-5}$. In agreement with the error estimation theory of the finite element method (see, for example, [26] and the references therein) the numerical scheme is of order 2 (resp. 1) in space when the L^2-norm (resp. H^1-norm) is considered.

discretization	number of	absolute error ($\varepsilon = 1$)		absolute error ($\varepsilon = 10^{-3}$)	
($N_x \times N_y$)	elements	L^2-norm	H^1-norm	L^2-norm	H^1-norm
16×16	450	1.754×10^{-4}	5.586×10^{-4}	9.668×10^{-6}	1.600×10^{-4}
32×32	1 922	4.138×10^{-5}	2.678×10^{-4}	2.392×10^{-6}	5.837×10^{-5}
64×64	7 938	1.003×10^{-5}	1.283×10^{-4}	5.790×10^{-7}	3.157×10^{-5}
128×128	32 258	2.466×10^{-6}	6.371×10^{-5}	1.327×10^{-7}	1.570×10^{-5}
256×256	130 050	6.126×10^{-7}	3.199×10^{-5}	3.768×10^{-8}	7.764×10^{-6}
512×512	522 242	1.676×10^{-7}	1.671×10^{-5}	1.000×10^{-8}	3.912×10^{-6}
1024×1024	2 093 058	4.412×10^{-8}	7.263×10^{-6}	2.616×10^{-9}	1.823×10^{-6}

discretization	number of	absolute error ($\varepsilon = 10^{-6}$)		absolute error ($\varepsilon = 10^{-9}$)	
($N_x \times N_y$)	elements	L^2-norm	H^1-norm	L^2-norm	H^1-norm
16×16	450	2.654×10^{-8}	8.099×10^{-6}	3.017×10^{-11}	3.140×10^{-6}
32×32	1 922	7.373×10^{-9}	2.384×10^{-6}	8.158×10^{-12}	8.340×10^{-7}
64×64	7 938	1.929×10^{-9}	6.096×10^{-7}	2.029×10^{-12}	2.151×10^{-7}
128×128	32 258	4.512×10^{-10}	1.459×10^{-7}	5.233×10^{-13}	5.888×10^{-8}
256×256	130 050	1.129×10^{-10}	4.117×10^{-8}	1.472×10^{-13}	1.661×10^{-8}
512×512	522 242	3.269×10^{-11}	1.123×10^{-8}	4.003×10^{-14}	4.806×10^{-9}
1024×1024	2 093 058	9.745×10^{-12}	2.802×10^{-9}	1.079×10^{-14}	1.240×10^{-9}

Table 1: L^2- and H^1-norms of the errors between the time-dependent exact solution (4.13) with $c_1 = c_2 = 1$, $c_3 = 10$ and the numerical solutions obtained with the AP scheme for various space mesh-sizes ($\Delta t = 10^{-5}$, $t = 0.1$) and four different values of ε.

In a similar fashion, the L^2-norms and the H^1-norms of the errors between the time-dependent exact solution and the numerical ones at $t = 0.1$ are given in Table 2 for various time steps Δt and a fixed mesh size ($N_x \times N_y = 64 \times 64$), for the same sets of parameters as those in Table 1. In this case, it is easily seen that the numerical scheme is of order 1 in time, as expected.

Comparison of the numerical results with a steady exact solution

In order to further validate the AP scheme, a comparison similar to the previous one has been carried out also for the steady non-linear problem (4.12). In this case, an exact solution has been obtained starting from the time-dependent solution (4.13), still assuming that the magnetic field is aligned with the x-axis and computing the source term f. This solution reads

$$T = c_1 + c_2 \left(\sin(\pi y) + \varepsilon \cos(2\pi x) \sin(\pi y) \right), \tag{4.14}$$

and is compared to the numerical resolutions obtained via the AP scheme making use of various mesh sizes, as done for the time-dependent problem, under the same choice

discretization (N_t)	time step (Δt)	absolute error ($\varepsilon = 1$) L^2-norm	H^1-norm	absolute error ($\varepsilon = 10^{-3}$) L^2-norm	H^1-norm
16	6.2500×10^{-3}	1.128×10^{-2}	6.832×10^{-2}	6.127×10^{-5}	2.807×10^{-3}
32	3.1250×10^{-3}	5.687×10^{-3}	4.019×10^{-2}	3.017×10^{-5}	1.466×10^{-3}
64	1.5625×10^{-3}	2.839×10^{-3}	2.350×10^{-2}	1.486×10^{-5}	7.727×10^{-4}
128	7.8125×10^{-4}	1.403×10^{-3}	1.306×10^{-2}	7.265×10^{-6}	4.061×10^{-4}
256	3.9063×10^{-4}	6.841×10^{-4}	6.577×10^{-3}	3.634×10^{-6}	2.054×10^{-4}

discretization (N_t)	time step (Δt)	absolute error ($\varepsilon = 10^{-6}$) L^2-norm	H^1-norm	absolute error ($\varepsilon = 10^{-9}$) L^2-norm	H^1-norm
16	6.2500×10^{-3}	5.731×10^{-9}	1.729×10^{-6}	6.541×10^{-12}	7.338×10^{-7}
32	3.1250×10^{-3}	3.184×10^{-9}	1.018×10^{-6}	3.852×10^{-12}	4.157×10^{-7}
64	1.5625×10^{-3}	1.749×10^{-9}	5.331×10^{-7}	1.906×10^{-12}	2.216×10^{-7}
128	7.8125×10^{-4}	7.680×10^{-10}	2.449×10^{-7}	1.015×10^{-12}	1.255×10^{-7}
256	3.9063×10^{-4}	3.849×10^{-10}	1.328×10^{-7}	5.474×10^{-13}	7.153×10^{-8}

Table 2: L^2-norms and H^1-norms of the errors between the time-dependent exact solution (4.13) with $c_1 = c_2 = 1$, $c_3 = 10$ and the numerical solutions obtained with the AP scheme for various time-steps Δt ($t = 0.1$, $N_x \times N_y = 64 \times 64$) and four values of ε.

as before of the parameters c_1, c_2 and ε. The results, given in Table 3, show that even when solving the non-linear elliptic problem (4.12), the expectations regarding the order of the method are fulfilled.

4.2 Comparison of the numerical results obtained by means of the AP and SP formulations

Since the main drawback of standard schemes (i.e. schemes based on the SP formulation) for the numerical resolution of highly anisotropic problems is connected to the ill-conditioning of the matrices to be inverted, we shall check in this section the asymptotic-preserving property of the AP reformulation, in particular the precise resolution of the problem independently on the parameter ε.

The evolution of the temperature distribution has been calculated on a rectangular domain $\Omega = [0, 1] \times [0, 1]$, by solving the problem (4.9) with the choice of parameters as given in (4.10) and (4.11). In order to fully determine the problem, the parameter γ, the initial temperature distribution T_0, and the magnetic field (given through the vectorial field b), must be fixed.

As far as the parameter γ is concerned, we took the value recommended by the physical experiments of a magnetically confined plasma, i.e. $\gamma = 9/2$ for ions and $\gamma = 5/2$ for electrons [28]. The initial temperature distribution T_0 has been chosen, for both ions and electrons, under the form of a Gaussian-shaped hot spot placed in the center of the domain:

$$T_0(x, y) = \frac{1}{2}\left(1 + 3\exp\left(-5\left(x - \frac{1}{2}\right)^2 - 5\left(y - \frac{1}{2}\right)^2\right)\right). \tag{4.15}$$

discretization	number of	absolute error ($\varepsilon = 1$)		absolute error ($\varepsilon = 10^{-3}$)	
$(N_x \times N_y)$	elements	L^2-norm	H^1-norm	L^2-norm	H^1-norm
16×16	450	1.091×10^{-2}	5.783×10^{-1}	1.012×10^{-5}	1.602×10^{-1}
32×32	1 922	2.585×10^{-3}	2.688×10^{-1}	2.604×10^{-6}	5.842×10^{-2}
64×64	7 938	6.277×10^{-4}	1.288×10^{-1}	6.516×10^{-7}	3.160×10^{-2}
128×128	32 258	1.546×10^{-4}	6.387×10^{-2}	1.620×10^{-7}	1.572×10^{-2}
256×256	130 050	3.835×10^{-5}	3.210×10^{-2}	4.029×10^{-8}	6.740×10^{-3}
512×512	522 242	9.549×10^{-6}	1.673×10^{-2}	1.004×10^{-8}	3.516×10^{-3}
1024×1024	2 093 058	2.382×10^{-6}	7.275×10^{-3}	2.594×10^{-9}	1.871×10^{-3}

discretization	number of	absolute error ($\varepsilon = 10^{-6}$)		absolute error ($\varepsilon = 10^{-9}$)	
$(N_x \times N_y)$	elements	L^2-norm	H^1-norm	L^2-norm	H^1-norm
16×16	450	8.333×10^{-7}	2.334×10^{-3}	9.017×10^{-10}	2.987×10^{-5}
32×32	1 922	2.315×10^{-7}	6.867×10^{-4}	2.438×10^{-10}	7.934×10^{-6}
64×64	7 938	6.059×10^{-8}	1.758×10^{-4}	6.064×10^{-11}	2.047×10^{-6}
128×128	32 258	1.417×10^{-8}	4.207×10^{-5}	1.564×10^{-11}	5.601×10^{-7}
256×256	130 050	3.546×10^{-9}	1.187×10^{-5}	4.399×10^{-12}	1.580×10^{-7}
512×512	522 242	1.026×10^{-9}	3.237×10^{-6}	1.196×10^{-12}	4.572×10^{-8}
1024×1024	2 093 058	3.059×10^{-10}	8.076×10^{-7}	3.224×10^{-13}	1.180×10^{-8}

Table 3: L^2-norms and H^1-norms of the errors between the steady exact solution (4.14) with $c_1 = c_2 = 1$ and the numerical solutions obtained with the AP scheme for various mesh sizes and four values of ε.

Concerning the choice of the magnetic field, the non-homogeneous field constructed in [17] has been selected. The direction of the magnetic field, given by the unit vector b is graphically represented in Fig. 4(a) and is given as follows:

$$b = B/|B|, \quad B = \left(3\left(2y-1\right)\cos\left(\pi x\right) + \pi, 3\pi y\left(y-1\right)\sin\left(\pi x\right)\right). \tag{4.16}$$

The condition numbers of the matrix to be inverted at each time step when solving the problem (i.e. the matrix Λ introduced in Section 3.3) via the AP scheme, resp. SP scheme, have been estimated[2] for several values of ε and a fixed mesh size and time ($N_x \times N_y = 64 \times 64$, $\Delta t = 10^{-2}$). These results, graphically shown in Fig. 3, clearly assert how, in the case of the SP scheme, the condition number of the matrices dramatically increases as the perturbation parameter decreases, leading – as a matter of fact – to unreliable numerical results and eventually to a break down of the scheme. By contrast, when the AP scheme is adopted, the condition numbers of the matrices are independent on ε, as the latter goes to zero.

In order to further compare the performances of the AP and SP schemes, the errors between the numerical results and a suitable *reference solution* are investigated for various values of the perturbation parameter ε. Since for the case under examination no analytical solution is available, the *reference solution* is defined as the numerical

[2]For this purpose, the subroutine provided by the LAPACK library has been used.

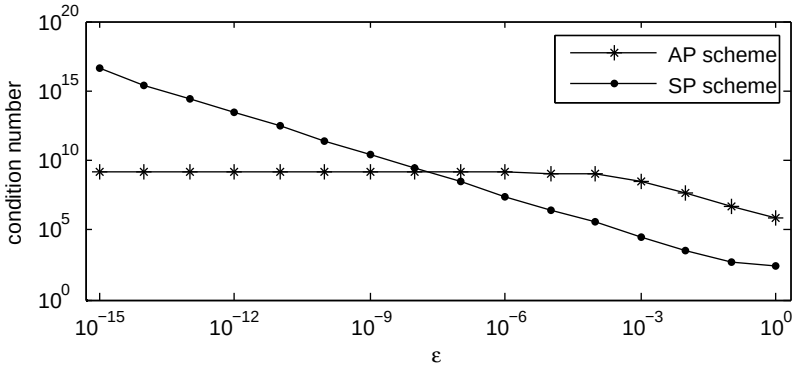

Figure 3: Estimate for the condition number of matrices involved in the algebraic linear systems to be solved (the values have been calculated in the reference case described in Section 4.3; $N_x \times N_y = 64 \times 64$, $\Delta t = 10^{-2}$, $t = 0.1$).

solution obtained via the AP scheme on a very fine mesh of $N_x \times N_y = 1024 \times 1024$, $\Delta t = 10^{-3}$.

The results, given in Table 4, show that both the L^2-norm and the H^1-norm of the absolute error associated to the AP scheme are independent on ε, as the latter tends to zero.

	absolute error, L^2-norm		absolute error, H^1-norm	
ε	AP scheme	SP scheme	AP scheme	SP scheme
10^0	2.902×10^{-3}	2.902×10^{-3}	7.351×10^{-2}	7.352×10^{-2}
10^{-3}	5.153×10^{-4}	4.231×10^{-2}	9.786×10^{-3}	4.360×10^{-2}
10^{-9}	4.898×10^{-4}	$*$	8.808×10^{-3}	$*$
10^{-15}	4.898×10^{-4}	$*$	8.808×10^{-3}	$*$

Table 4: L^2- and H^1-norms of the errors at $t = 0.1$ between a reference solution (obtained on a fine mesh of $N_x \times N_y = 1024 \times 1024$, $\Delta t = 10^{-3}$) and the numerical solutions obtained via the AP and SP schemes for different values of ε and $\Delta t = 10^{-2}$, $N_x \times N_y = 64 \times 64$. The symbol $*$ appears when no meaningful solutions are obtained.

In Table 4, one can remark that the errors of the SP scheme are missing for the cases with $\varepsilon = 10^{-9}$ and $\varepsilon = 10^{-15}$. This is due to the fact that for *very small* ε the SP scheme does not converge any more. Indeed, in these cases, the iterative procedure carried out at each time step in order to solve the non-linear problem, had to be stopped because the sequence $T^{n,k}$ failed to converge towards the fixed point T^{n+1} (see Sec. 3.1). This numerical difficulty, which – according to all the calculations performed so far – does not affect the AP scheme, makes the AP scheme the only reliable choice when $\varepsilon \ll 1$.

Another interesting aspect to be studied when comparing both schemes is the simulation time. In the case with $\varepsilon = 10^{-3}$ given in Table 4, for which the SP scheme provides a reliable solution, it is interesting to observe that in order to obtain with the SP scheme a numerical solution equally precise as the AP results (approximatively 5×10^{-4}), it is necessary to chose a mesh of $N_x \times N_y = 128 \times 128$ and $\Delta t = 2.5 \times 10^{-3}$. This requires

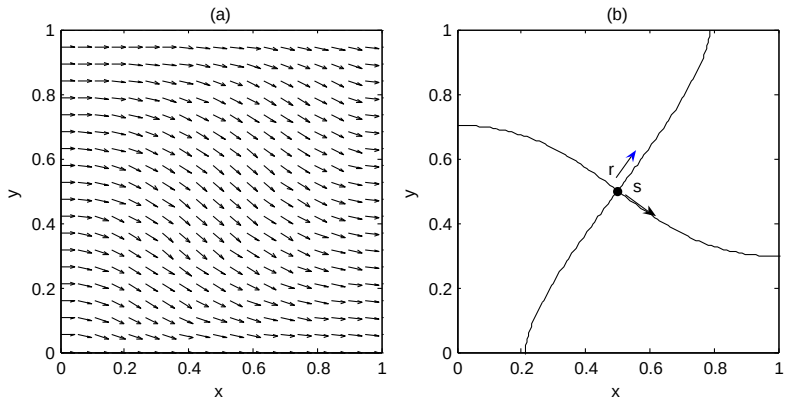

Figure 4: (a) Vector field b, representing the direction of the magnetic field; (b) Graphical representation of the s–direction and r–direction, i.e. the directions parallel resp. perpendicular to the field b and passing through the center of the domain Ω.

a SP computational time more than ten times larger than the AP computational time. Again the considerable advantage of the AP technique is underlined.

4.3 Study of the temperature evolution in a magnetically confined plasma

In the present section, we present some numerical results concerning the application of the AP methodology to the model equation of the temperature evolution in a magnetically confined plasma, described in Section 2. The choice of the parameter γ, of the magnetic field b and of the initial temperature profile T_0 have been previously described in Section 4.2. It should be stressed here that nor this initial temperature T_0, nor this magnetic field direction b, have a specific physical meaning. Computations involving different initial temperature distributions have been carried out but, since the choice of T_0 does not seem to alter qualitatively the results and the considerations that will be outlined in the following, we focus only on the results obtained using the choice of T_0 given in Eq. (4.15). The magnetic field direction given in Eq. (4.16) has been chosen since it satisfies the requirement of being a non homogeneous field; nevertheless such a choice is not restrictive and any realistic magnetic field direction could be considered as well. The only free parameter of the problem is thus the quantity ε.

In the following, we investigate the effects on T of changing the parameter ε on a fixed grid. For this, it is useful to introduce two specific directions, which we shall call s and r, defined as follows. The direction s is taken as the direction along the streamline of the vector field b passing through the point $(x_c, y_c) = (0.5, 0.5)$, and the direction r is obtained as the direction locally perpendicular to the streamlines of the vector field b passing though the point (x_c, y_c). The direction s and r, which are shown in Fig. 4(b) – for the case of the vector field given in (4.16) – may be addressed, respectively, as the *parallel* and *perpendicular directions*.

The evolution of the temperature has been obtained for several values of the param-

eter ε. A representative selection of these results, namely the temperature distribution in the domain Ω at four specific time instants ($t = 0.01,\ 0.05,\ 0.1,\ 10$) is given in Fig. 5 and Fig. 6 in the case of ions ($\gamma = 9/2$) for $\varepsilon = 1, 10^{-3}, 10^{-15}$ and in the case of electrons ($\gamma = 5/2$) for $\varepsilon = 10^{-15}$.

From all the shown temperature field evolutions, it is remarkable how the parallel direction, s, is actually the privileged direction – in terms of diffusion of the temperature – for *sufficiently small* times, and for any value of the parameter ε, except $\varepsilon = 1$. As a general rule, the maximum temperature decreases in time as a consequence of the absence of any energy source and of the specific boundary conditions imposing null or outgoing energy fluxes (see Eq. (2.2)). In the case of ions, the monotonic decrease (towards zero) of the maximum temperature in time can be remarked in the temperature distributions given in Fig. 5 and Fig. 6(a–d). This decrease is responsible for an outstanding behavior of the diffusion process: as the temperature becomes smaller and smaller, the parallel diffusion coefficient, $\mathcal{K}_\parallel = K_\parallel T^{5/2}$, becomes also smaller and smaller, leading to a loss of predominance of the diffusion in the parallel direction with respect to the diffusion in the perpendicular direction, which is independent on the temperature. This behavior, which is intrinsic to the problem itself and is not dependent on the initial temperature distribution, is only partially contrasted by small values of the parameter ε: The smaller is ε, the slower is the loosing of predominance of the parallel diffusion, but as time lapses it necessarily takes place. It should be stressed, however, that this phenomenon is concomitant to the already mentioned decay of the overall ion temperature field, which tends to zero over all the computational domain, as it may be seen, for instance, in Figs. 5(d,h) and Fig. 6(d). In this regard, it may be added that the decrease of the overall ion temperature towards zero and its associated numerical/mathematical difficulties, may not occur in realistic magnetically confined plasma simulation, due to the presence of source terms keeping the temperature approximately at the same level.

In the case of electrons, a similar discussion may be repeated, with the difference that in this case the overall temperature approaches an equilibrium value which is not zero, as shown in Fig. 6(h). This remarkable difference with respect to the case of ions is due to the fact that for the electrons ($\gamma = 5/2$), the boundary conditions provide a null energy flux on the whole boundary Γ of the computational domain, while for the ions ($\gamma = 9/2$) an outgoing energy flux is imposed on Γ_N.

In Fig. 7, the L^∞-norm and the L^2-norm of the ion and electron temperature fields are plotted as functions of time. For both ions and electrons, the decrease of the L^∞ norms clearly underlines the phenomenon mentioned above. For what concerns the L^2 norm, its monotonic decrease in the case of ions and its constant value (within numerical errors) in the case of electrons are in agreement with the results shown in Fig. 5 and in Fig. 6 previously discussed. In the case of ions, as already stressed, the numerical calculations cannot be carried out up to an indefinite time because the values of the temperature in some portions of Ω will sooner or later becomes so small that numerical difficulties arise[3]; they have been stopped here at $t = 4$, making use of $\Delta t = 10^{-3}$.

[3]When the temperature becomes of the same order of magnitude as the *machine precision*, it can accidentally become negative in some portions of the computational domain, thus leading to meaningless numerical results and finally to a breakdown of the numerical scheme.

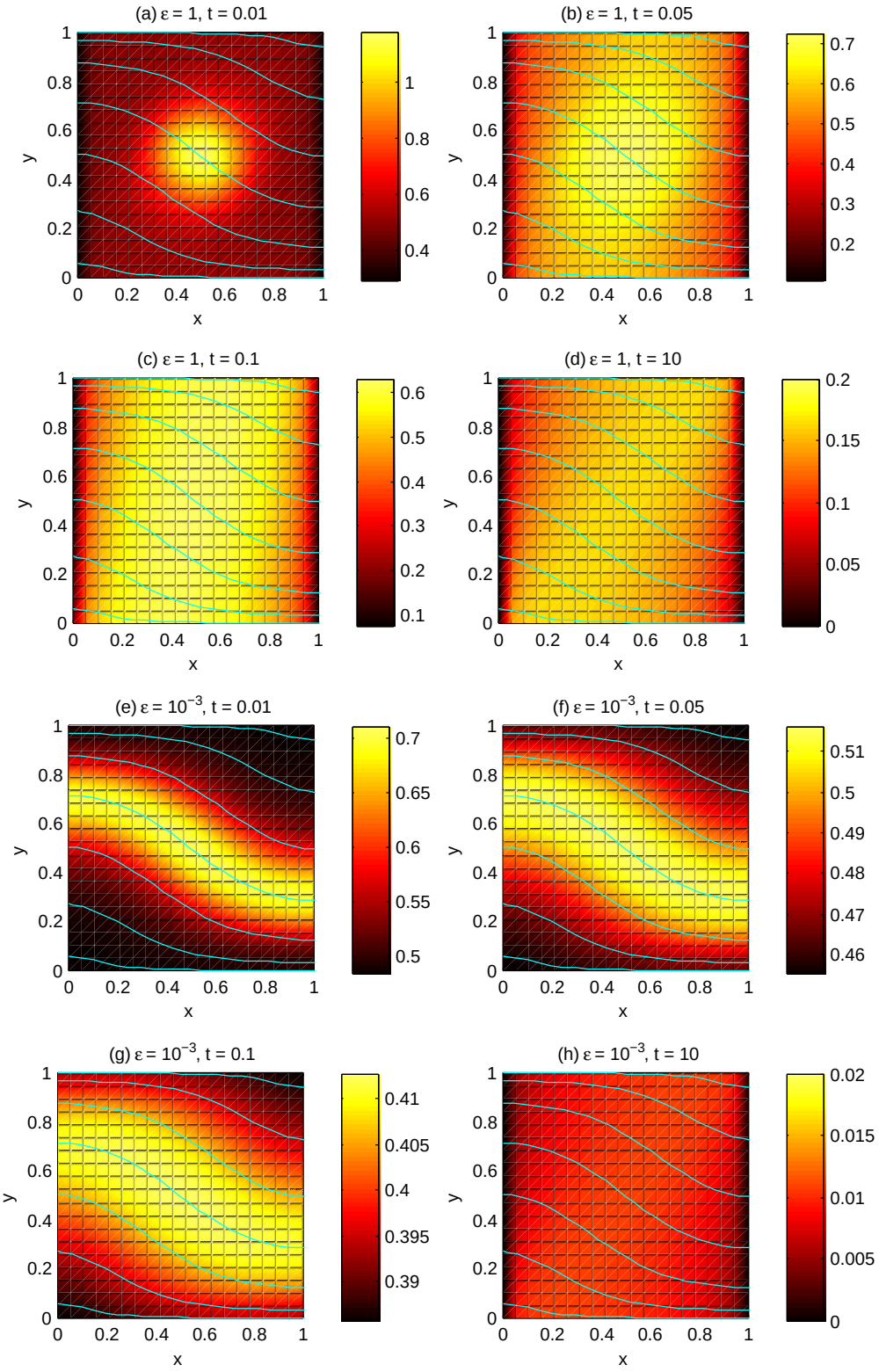

Figure 5: Ion temperature distribution $T_i(x, y)$ and streamlines of the vector field b obtained with $\varepsilon = 1$ (a–d) and $\varepsilon = 10^{-3}$ (e–h) at $t = 0.01$, $t = 0.05$, $t = 0.1$ and $t = 10$ ($\Delta t = 10^{-2}$, $N_x = N_y = 64$).

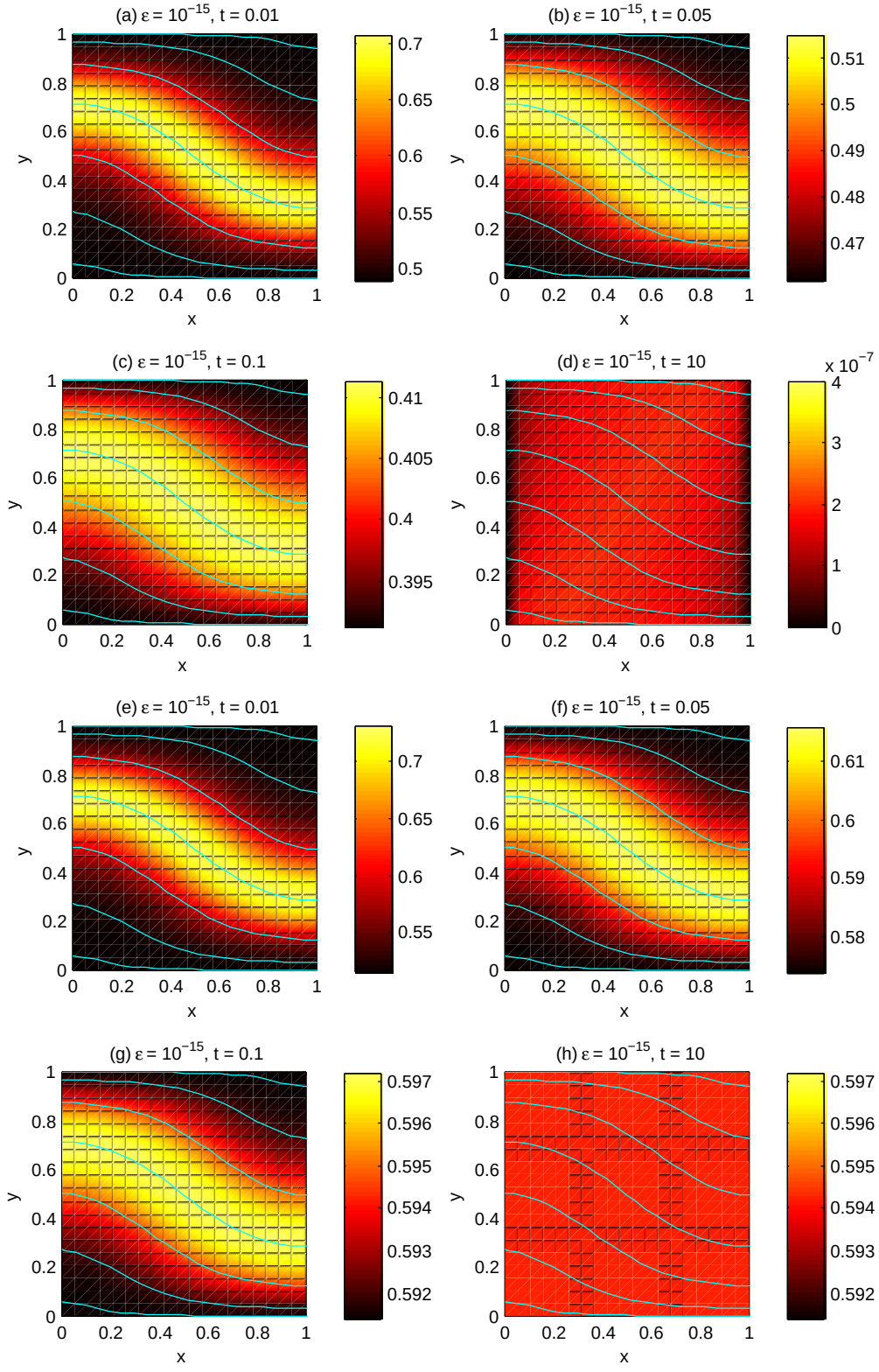

Figure 6: Ion (a–d) $T_i(x, y)$ and electron (e–h) $T_e(x, y)$ temperature distribution and streamlines of the vector field b obtained with $\varepsilon = 10^{-15}$ at $t = 0.01$, $t = 0.05$, $t = 0.1$ and $t = 10$ ($\Delta t = 10^{-2}$, $N_x = N_y = 64$).

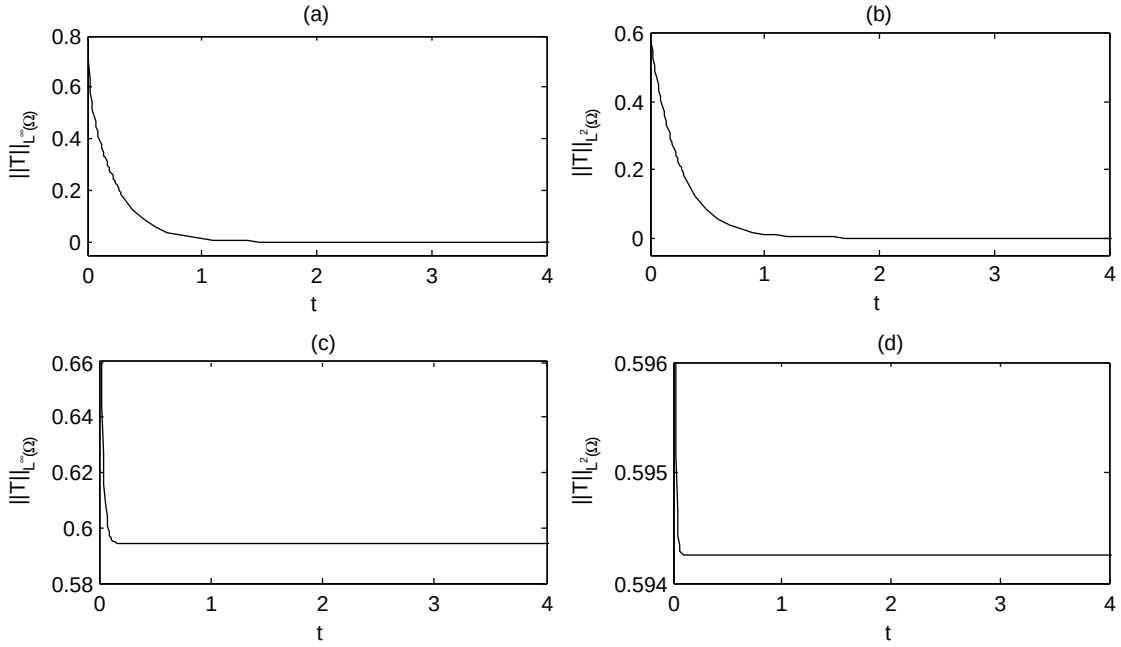

Figure 7: L^∞-norm and L^2-norm of the temperature of ions (a,b) and electrons (c,d) in the domain Ω as a function of time ($\varepsilon = 10^{-6}$).

When investigating the role of the value of the parameter ε on the parallel and perpendicular diffusion processes, it may be interesting to analyze the temperature profiles at a fixed time t along the parallel and perpendicular directions, respectively named s and r, which are graphically represented in Fig. 4(b). These ion and electron temperature profiles obtained for several values of ε are shown in Fig. 8. These results are extracted from the time evolution of the temperature, fixing $t = 0.05$, in order to guarantee that the temperature fields have not reached too small values which prevents from numerical errors.

As expected, the temperature profiles along the parallel direction (s-direction) are almost flat, excepting the case with $\varepsilon = 10^{-3}$. For this latter value of ε, in fact, the diffusion in the parallel direction is not *sufficient* to lead in the fixed time interval to a uniform distribution of the temperature along the s-direction, while in all other cases, the parallel diffusion is so *large* as to lead to an almost uniform temperature distribution.

From the analysis of the temperature distribution along the perpendicular direction (r-direction), it is easily seen that no appreciable change occurs as ε gets smaller than $\varepsilon = 10^{-3}$, as for the profiles along the s-direction. Indeed, as the parameter ε gets smaller and smaller, its impact on the temperature distribution gets less and less important, as expected.

Finally, with the aim of checking the mesh sensitivity of the AP numerical results, the comparison of the ion temperature profiles along the s and r directions are shown in Fig. 9, as computed with several meshes and a fixed time step Δt. In order to compare these results with those obtained making use of classical methods, the profiles obtained with the SP scheme are given as well. It easily seen that, with the AP scheme, the dependence of the numerical results on the mesh size becomes barely appreciable as the

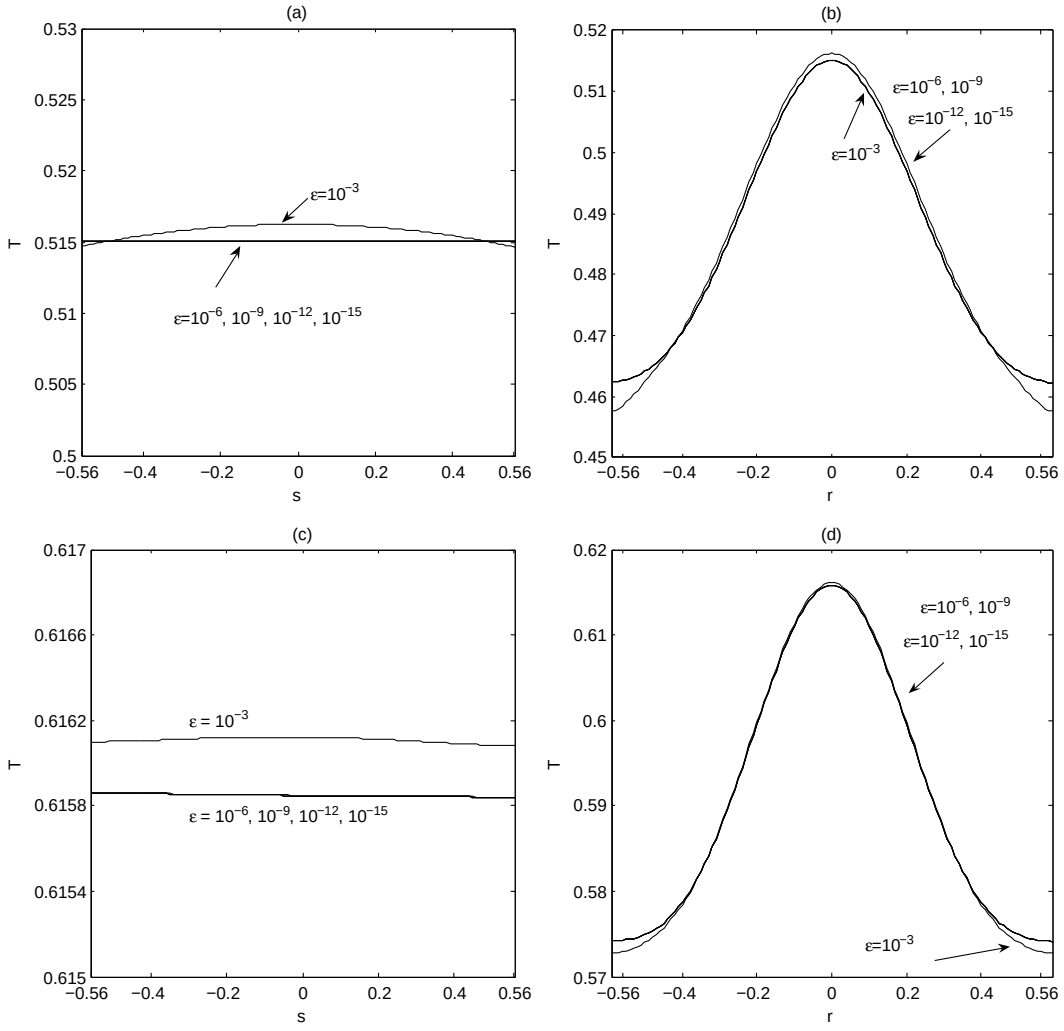

Figure 8: Ion (a,b) and electron (c,d) temperature profiles along the s–direction and the r–direction obtained for various values of the parameter ε, at $t = 0.05$ ($N_x \times N_y = 128 \times 128$, $\Delta t = 10^{-3}$).

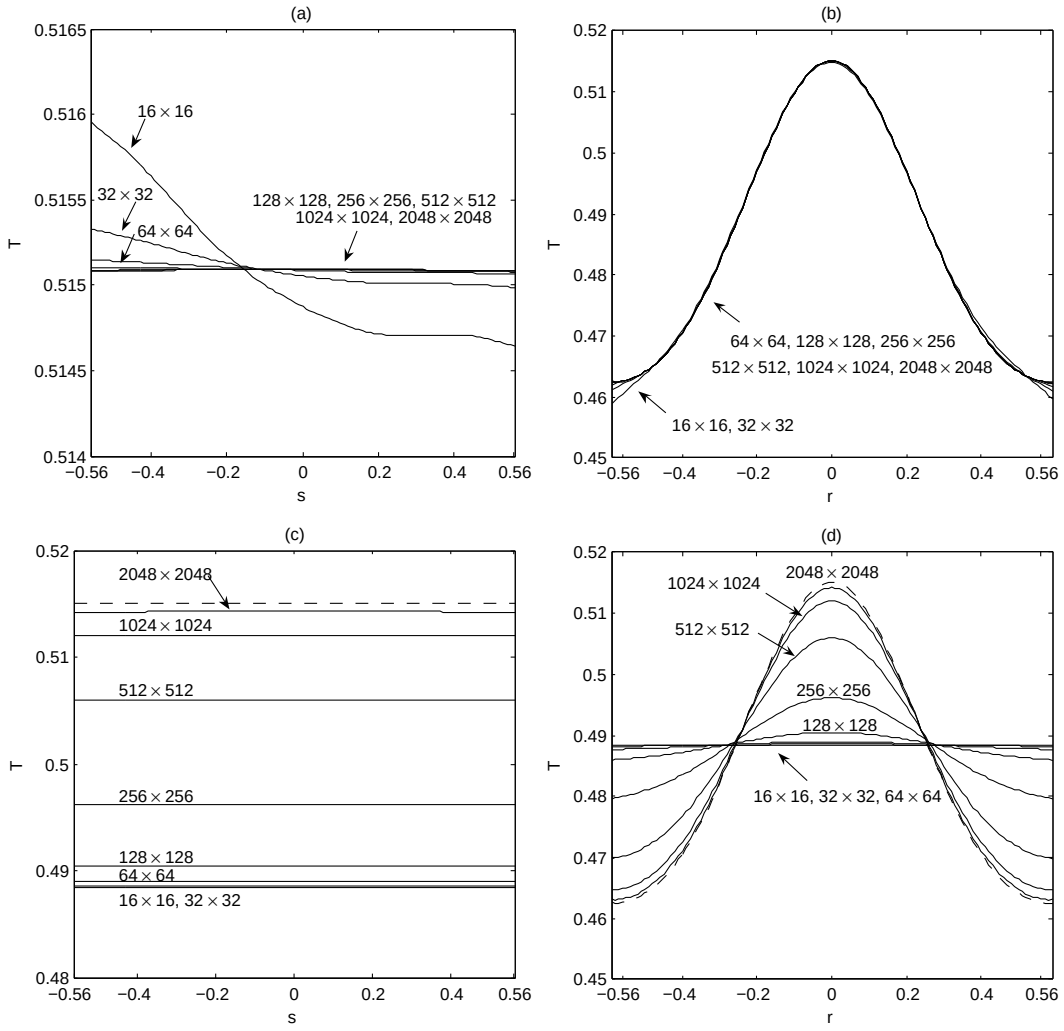

Figure 9: Ion temperature profile along the s and r–directions obtained for $\varepsilon = 10^{-6}$ and various mesh sizes with the AP scheme (a,b) and the SP scheme (c,d) at $t = 0.1$ ($\Delta t = 2.5 \times 10^{-2}$). The dashed profiles in (c) and (d) represent the reference solution (obtained with the AP scheme on the fine mesh, $N_x \times N_y = 2048 \times 2048$, $\Delta t = 10^{-2}$).

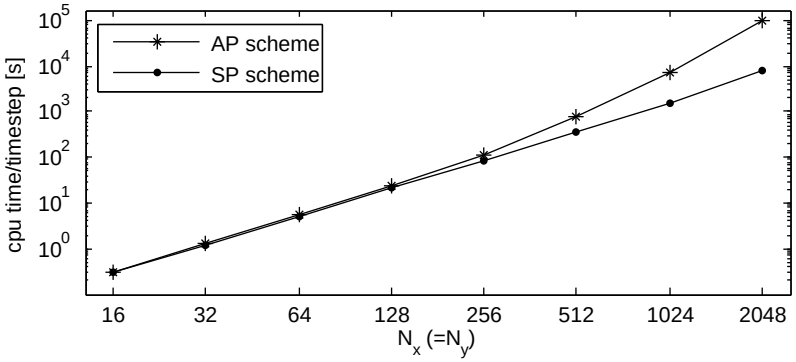

Figure 10: CPU time (for one time step) required by the AP and SP schemes to compute the solutions plotted in Fig. 9 ($\Delta t = 2.5 \times 10^{-2}$).

mesh size increases, while very thick meshes are to be used in order to get a comparable degree of accuracy with the SP scheme.

In order to compare the computational burden associated to the solutions plotted in Fig. 9, the CPU time required to obtain the solutions for each time step are given in Fig. 10. For a given mesh size, the AP scheme is clearly more computationally expensive than the SP scheme, as explained in Section 3; nevertheless, taking into account that – as seen above – the AP scheme provides good results with coarser meshes than those required by the SP scheme, it turns out that the AP scheme is clearly less expensive in terms of both CPU time and data storage.

5 Conclusions

An asymptotic-preserving (AP) scheme has been introduced and implemented for the numerical resolution of the simplified temperature equation model of a magnetically confined plasma – which is a non-linear evolution problem characterized by highly anisotropic diffusion. This scheme generalizes the asymptotic-preserving scheme developed in a previous work [17] for linear elliptic problems, to the present non-linear evolutive case.

The here proposed AP scheme is shown to be much more performant than standard discretization schemes based on the singular perturbation (SP) formulation. In particular, it is shown that the condition number of the discretization matrix, as well as the errors, are ε-independent in the AP case, which is the essential feature of AP schemes. Standard schemes would need an ε-dependent grid in order to be accurate.

Another important advantage of the here presented AP scheme is that the mesh has not to be adapted to the direction of the anisotropy: coarse Cartesian grids are generally sufficient to get accurate results even when extremely high anisotropies are involved (i.e. $\varepsilon \ll 1$), while SP scheme may require far more computationally expensive discretization in order to provide the same degree of accuracy.

The here proposed AP scheme turns out to be an excellent candidate for the numerical treatment of magnetically confined plasmas, for which extremely high anisotropic

diffusion is involved and meshes independent from the direction of the anisotropy are desirable.

Acknowledgments

This work has been supported by the ANR project ESPOIR (Edge Simulation of the Physics Of Iter Relevant turbulent transport, 2009-2013) and ANR project BOOST (Building the future Of numerical methOdS for iTer, 2010-2014). One of the authors (A.M.) has been supported by CNRS (contrat No. 244516).

References

[1] S. N. Antontsev, S. I. Shmarev, *A model porous medium equation with variable exponent of nonlinearity: existence, uniqueness and localization properties of solutions*, Nonlinear Anal.-Theor. **60**, 3, 515–545 (2005)

[2] S. F. Ashby, W. J. Bosl, R. D. Falgout, S. G. Smith, A. F. Tompson, T. J. Williams, *A Numerical Simulation of Groundwater Flow and Contaminant Transport on the CRAY T3D and C90 Supercomputers*, Int. J. High Perform. Comput. Appl. **13**, 1, 80–93 (1999)

[3] P. Basser, D. K. Jones, *Diffusion-tensor MRI: theory, experimental design and data analysis – a technical review*, NMB Biomed. **15**, 7/8, 456–467 (2002)

[4] C. Beaulieu, *The basis of anisotropic water diffusion in the nervous system – A technical review*, NMR Biomed. **15**, 7/8, 435–455 (2002)

[5] M. Bennoune, M. Lemou, L. Mieussens, *Uniformly stable numerical schemes for the Boltzmann equation preserving the compressible Navier-Stokes asymptotics*, J. Comput. Phys. **227**, 8, 3781–3803 (2008)

[6] B. Berkowitz, *Characterizing flow and transport in fractured geological media: A review*, Adv. Water Resour. **25**, 8/12, 861–884 (2002)

[7] L. Boccardo, A. Dall'Aglio, T. Gallouët, L. Orsina, *Existence and regularity results for some nonlinear parabolic equations*, Adv. Math. Sci. Appl. **9**, 2, 1017–1031 (1999)

[8] S. Brull, P. Degond, F. Deluzet, A. Mouton, *Asymptotic-Preserving scheme for a bi-fluid Euler-Lorentz model*, ArXiv:1104.3339v1 [math-ph]

[9] P. Crispel, P. Degond, M-H. Vignal, *An asymptotic preserving scheme for the two-fluid Euler-Poisson model in the quasineutral limit*, J. Comp. Phys. *223*, 1, 208–234 (2007)

[10] N. Crouseilles, M. Lemou, *An asymptotic preserving scheme based on a micro-macro decomposition for collisional Vlasov equations: diffusion and high-field scaling limits*, Kinetic and Related Models **4**, 2, 441–477 (2011)

[11] T. A. Davis, *A column pre-ordering strategy for the unsymmetric-pattern multifrontal method*, ACM T. Math. Software **30**, 2, 165–195 (2004)

[12] T. A. Davis, *Algorithm 832: UMFPACK, an unsymmetric-pattern multifrontal method*, ACM T. Math. Software **30**, 2, 196–199 (2004)

[13] T. A. Davis, I. S. Duff, *A combined unifrontal/multifrontal method for unsymmetric sparse matrices*, ACM T. Math. Software **25**, 1, 1–19 (1999)

[14] T. A. Davis, I. S. Duff, *An unsymmetric-pattern multifrontal method for sparse LU factorization*, SIAM J. Matrix Anal. Appl. **18**, 1, 140–158 (1997)

[15] P. Degond, *Asymptotic-Preserving Schemes for Fluid Models of Plasmas*, arXiv:1104.1869v1 [math-ph] (2011)

[16] P. Degond, F. Deluzet, D. Savelief, *Numerical approximation of the Euler-Maxwell model in the quasineutral limit*, J. Comput. Phys. **231**, 4, 1917–1946 (2012)

[17] P. Degond, A. Lozinski, J. Narski, C. Negulescu, *An asymptotic-preserving method for highly anisotropic elliptic equations based on a micro–macro decomposition*, J. Comput. Phys. **231** (2012), no. 7, 2724-2740.

[18] F. Filbet, C. Negulescu, C. Yang, *Numerical study of a nonlinear heat equation for plasma physics*, to appear in International J. of Comp. Maths.

[19] T. Y. Hou, X.-H. Wu, *A multiscale finite element method for elliptic problems in composite materials and porous media*, J. Comput. Phys. **134**, 1, 169–189 (1997)

[20] J. D. Huba, *NRL Plasma Formulary*, Beam Physics Branch/Plasma Physics Division, Naval Research Laboratory, Washington DC (2007)

[21] L. Isoardi, *Modélisation du transport dans le plasma de bord d'un tokamak*, Thèse de doctorat de l'Université Paul Cézanne Aix-Marseille II (2010)

[22] C. Johnson, *Numerical Solution of Partial Differential Equations by the Finite Element Method*, Cambridge University Press, Cambridge (1987)

[23] S. Jin, *Efficient Asymptotic-Preserving (AP) Schemes for Some Multiscale Kinetic Equations*, SIAM J. Sci. Comp. **21**, 441–454 (1999)

[24] M. Lemou, L. Mieussens, *A new Asymptotic-Preserving scheme based on micro-macro decomposition for linear kinetic equations in the diffusion limit*, SIAM J. Sci. Comput. **31**, 334–368 (2008)

[25] P. Perona, J. Malik, *Scale-space and edge detection using anisotropic diffusion*, IEEE Trans. Pattern Anal. Mach. Intell. **12**, 7, 629–639 (1990)

[26] I. Ramière, *Convergence analysis of the Q_1-finite element method for elliptic problems with non-boundary-fitted meshes*, Int. J. Numer. Meth. Engng. **75**, 1007–1052 (2008)

[27] P. Sharma, G. W. Hammett, A fast semi-implicit method for anisotropic diffusion, J. Comput. Phys. **230**, 12, 4899–4909 (2011)

[28] P. C. Stangeby, *The plasma boundary of magnetic fusion devices* (Chapter 2), IOP, University of Toronto, Canada (2000)

[29] J. L. Vazquez, *The Porous Medium Equation. Mathematical Theory*, Oxford University Press (2006)

[30] J. Weickert, *Anisotropic Diffusion in Image Processing*, Teubner, Stuttgart (1998)